technologies

Article

Design of Beam-Forming Networks for Fermat Spiral Antenna Arrays

Kleiverg Encino [1], Marco A. Panduro [1,*], Alberto Reyna [2], David H. Covarrubias [1] and Leopoldo A. Garza [2]

[1] CICESE Research Center, Electronics and Telecommunications Department, Carretera Ensenada-Tijuana No. 3918, Zona Playitas, Ensenada 22860, Baja California, Mexico; kleiverg@cicese.edu.mx (K.E.); dacoro@cicese.mx (D.H.C.)

[2] Electronics Department, Universidad Autónoma de Tamaulipas, UAMRR-R, Carretera Reynosa-San Fernando, Reynosa 88779, Tamaulipas, Mexico; alberto.reyna@docentes.uat.edu.mx (A.R.); leopoldo.garza@docentes.uat.edu.mx (L.A.G.)

* Correspondence: mpanduro@cicese.mx

Abstract

This paper presents a novel design technique using beam-forming networks based on CORPS (coherently radiating periodic structures) technology to achieve the simplification of the feed network of Fermat spiral antenna arrays. The use of one-layer CORPS structures generates the values of co-phasal excitation required for the feeding network system based on subarrays. The setting of subarrays has been achieved through the study of the behavior of phases of each antenna element in scanning. In this way, elements that exhibit linear behavior in scanning can be grouped. Furthermore, the geometry of the antenna array system using a Fermat spiral configuration applies methods for side lobe level (SLL) reduction such as: a raised cosine amplitude excitation and optimization of the amplitude excitations through the method of genetic algorithms (GA), CORPS amplitude distribution and uniform distribution. The contribution of this paper is to provide a design of a phased antenna system for a Fermat spiral array geometry considering the analysis and study in the performance of SLL, scanning range, and the phase shifters reduction. Full-wave electromagnetic results are provided for the full phased antenna system by using circular patch antenna elements at a frequency of 6 GHz. If our system using CORPS is compared with the use of a conventional feeding network where every antenna in the spiral array is fed with a phase shifter, the benefits of using this phased spiral array system are: a phase shifters reduction capability of 33%, steering ranges of $\pm 22^{\circ}$ in the elevation plane, low SLL using the proposed distribution techniques. Furthermore, the choice of CORPS 2×3 networks would allow the integration of the antenna system where one layer is proposed for the feeding network and another layer for the antenna array with the aim of avoiding crossings and unwanted radiation.

Keywords: Fermat spiral geometry; antenna system; beam-scanning; CORPS; side lobe level

Check for updates

Academic Editor: Sotirios K. Goudos

Received: 16 December 2025
Revised: 29 January 2026
Accepted: 30 January 2026
Published: 10 February 2026

1. Introduction

Phased array systems have allowed improvement of the performance of communication systems in different applications, such as satellites [1,2], mobile communications [3,4], radar [5–8], tracking [9–11], and 5G networks [12,13]. The use of antenna systems in these scenarios requires control of beam-steering in an electronically way to provide low side lobe level. Beam-forming networks are used to achieve this by providing the required amplitude and phase values, thus generating the desired radiation pattern.

It is well known that antenna arrays with aperiodic geometries allow the elimination of grating lobes. These are undesirable in applications requiring beam-steering and low side lobe levels such as those mentioned previously. Evolutionary optimization [14], particle swarm optimization [15], controlled random processes [16], and spatial tapering techniques, such as the Gaussian function [17] and the Taylor function [18], have been used to create aperiodic arrays. Furthermore, geometries inspired by nature have been proposed, for example the Fermat spiral [18–20]. This geometry has demonstrated in the state of the art that it provides a useful performance to avoid the appearance of grating lobes and to achieve a good SLL performance. Likewise, the evaluation of this spiral geometry is really simple and does not require a large calculation time, even with a high number of elements.

The configuration of the Fermat spiral has been analyzed in the previous literature in antenna arrays to be assessed in radiation performance. However, techniques of beam-forming and simplifying the feed network of this aperiodic array are scarce. This is because the beam-forming techniques conventionally used for periodic arrays are not enough for implementation in aperiodic arrays or spiral arrays. For instance, the sub-arrays technique [21] group elements with the same position on one of the plane axes, so that they can be fed with a single amplifier or phase shifter. However, in a spiral array, all the elements have completely different coordinates [22], and the required phase behavior is not progressive, unlike linear and planar array configurations. This generates a challenge of providing beam-forming networks for feeding antenna arrays in a Fermat spiral geometry and aperiodic array systems.

With the aim of developing the integration of the CORPS methodology with a spiral array, it is proposed to use one layer for the design of the feed network and another layer for the design of the antenna array. This integration would allow for more space for the feed network, thus avoiding crossing that could affect the performance of the antenna system. The integration presents a challenge, however, with the proposed methodology. The goal is to make the integration challenge less than the challenge that CORPS networks in spiral arrays are intended to solve.

Therefore, this paper proposes a new design technique for feeding Fermat spiral antenna arrays. The technique is based on the application of CORPS networks of one layer [23,24], specifically networks of two inputs and three outputs (CORPS 2×3). This paper analyses the phase requirements of the Fermat spiral array by evaluating the co-phasal excitation for this array structure to set an adequate beam-forming or feeding network. The case of CORPS 2×3 configuration generates a linear output phase slope which can be matched to the phase behavior of Fermat spiral array. Then, the required phase behavior of Fermat spiral arrays is studied and analyzed to set sub-groups that match several CORPS 2×3 networks.

As a result, the proposed design achieves a reduction of phase shifters used in the phased antenna system for this particular array structure. Furthermore, different amplitude distributions can be used to improve the performance of SLL. Genetic algorithms [25] and a raised cosine distribution have been adapted to the Fermat spiral array geometry and used to obtain low SLL in the phased antenna system. An evaluation and comparative assessment of these amplitude excitation techniques is provided in this study for phased spiral array systems.

The contribution of this paper is to provide a design of a phased antenna system for a Fermat spiral array geometry considering the analysis and study in the performance of SLL, scanning range, and the phase shifters reduction. Full-wave electromagnetic results are provided for the full phased antenna system by using circular patch antenna elements at a frequency of 6 GHz. The differences of the present study with respect to previous work are: the application of CORPS technology to a non-conventional geometry, like the Fermat spiral. Previous studies, e.g., [23], have consider the application of CORPS for linear and circular array geometries. Another novel contribution is the utilization of CORPS network to reduce the number of phase shifters, trying to make simpler systems or less complex beamforming networks for this kind of antenna array geometries. Furthermore, a comparative analysis of the application of different amplitude excitation techniques is provided for these spiral antenna array systems to have radiation characteristics of low SLL. If our system using CORPS is compared with the use of a conventional feeding network, where every antenna in the spiral array is fed with a phase shifter, the benefits of using this phased spiral array system are: a phase shifter's reduction capability of 33%, steering ranges of $\pm 22^\circ$ in the elevation plane, and low SLL using the proposed distribution techniques. The results are validated using a full-wave electromagnetic solver for an 18-element spiral array considering a scanning range of $\pm 22^\circ$ in elevation angle. The use of genetic algorithms and raised cosine amplitude provide a good SLL performance using electromagnetic solver to assess the phased spiral array model and to consider mutual coupling among elements. The designed Fermat spiral array could be considered a good design choice for phased antenna system applications.

2. Design of Phased Fermat Spiral

The choice of groups of elements in a spiral array antenna is achieved once the behavior of the phases in scanning has been analyzed and after that the possibility of using a CORPS configuration for the beam forming network is studied. The incorporation of the proposed CORPS networks and the spiral arrays achieves the reduction of phase shifters, and the use of amplitude distribution techniques allow the minimization of SLL.

2.1. CORPS Network Model

The traditional CORPS model consists of N inputs and M outputs, where the number of layers required for a network with these characteristics is M-N. Each layer is composed of splitting nodes S and recombination nodes R [23], as shown in the Figure 1. If more layers are used in a CORPS network, fewer control inputs are needed for the same number of outputs.

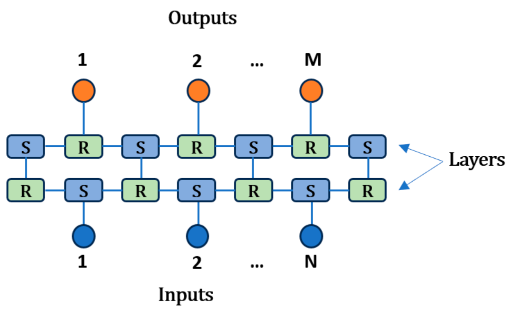

Figure 1. Traditional CORPS model.

Figure 2 shows the general structure of the S and R nodes. The split nodes, S, have one input port and N output ports. Each output port delivers the Nth part of the power introduced at the input port. The power delivered by the two ports for the case of a split node with two output ports is [23]:

$$W_s = \left(E_1{}^2 + E_2{}^2\right) G_s \tag{1}$$

where E_1 and E_2 are the magnitude of each of the output ports and G_s is the real part of the admittance seen at output ports. In an S-node case, each output will have the same phase shift as related to the phase of the input [23]. These nodes link the layers of a CORPS network.

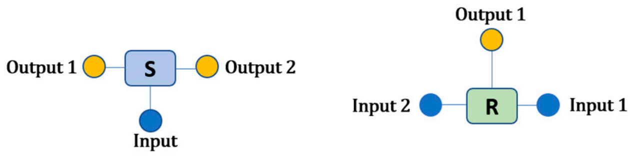

Figure 2. General structure of S and R nodes.

The R nodes have one output port and two input ports. Thus, the power at the output port can be calculated as [23]:

$$W_R = G_R\,(E_1{}^2 + E_2{}^2 + 2E_1E_2\cos(\theta_1 - \theta_2) \tag{2}$$

where E_1, E_2 and θ_1, θ_2 are the field magnitudes and phases of each of the input ports, and G_R is the admittance seen at output. The last term represents the correlation between input fields at R-node that depend on its arrival phase. Therefore, the amplitude of the resulting signal depends on the phase difference of the inputs. Maximum output amplitude is obtained when the phase difference is 0 and minimum amplitude is obtained when a phase difference is set to 180°.

On the other hand, it is clear that it is necessary to increase the number of layers in a CORPS network to decrease the number of phase shifters. However, it is pointed out in [24] that this increases the losses due to energy dissipation. Now, CORPS networks with two inputs and three outputs (one layer) have the characteristic of presenting a linear phase slope in scanning [26], as observed in Figure 3. This figure shows the behavior of output phases of CORPS networks with a fixed number of inputs (2) and a different number of outputs (3, 4, 5, and 6). The phases are normalized. It can be noted that the other configurations do not exhibit linear output behavior. Therefore, 2×3 CORPS networks (two inputs and three outputs) have been chosen to be integrated with a Fermat spiral array where elements exhibiting linear scanning behavior can be grouped to be fed with the outputs of these CORPS 2×3 networks.

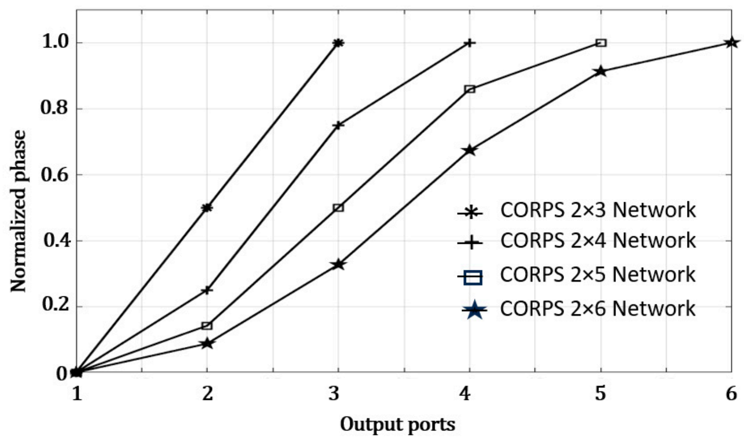

Figure 3. Phase slope for CORPS networks with different numbers of layers.

In a 2×3 network, if $[U]$ is the vector of complex inputs and $[C]$ represents the behavior of a 2×3 network, the output vector $[\mathrm{V}] = [V_1\ V_2\ V_3]$. is given as [23–27]:

$$[V] = [C][U]^T \tag{3}$$

where:

$$[U] = [U_1 U_2] \tag{4}$$

$$[C] = \begin{bmatrix} \frac{1}{\sqrt{2}} & 0 \\ \frac{1}{2} & \frac{1}{2} \\ 0 & \frac{1}{\sqrt{2}} \end{bmatrix} \tag{5}$$

Figure 4 shows the phase and amplitude behavior of CORPS 2×3 networks when a phase difference of 0 and 90° is set at input ports. It can be seen that the phase of the middle port corresponds to the arithmetic mean of the input ports phase. In the case of the amplitude, there is an attenuation that increases as the difference approaches 180°. This amplitude attenuation can be compensated by using a variable amplifier at the output port of each recombination node [28], or these output amplitudes can be used to directly feed the antenna elements, as considered in this study.

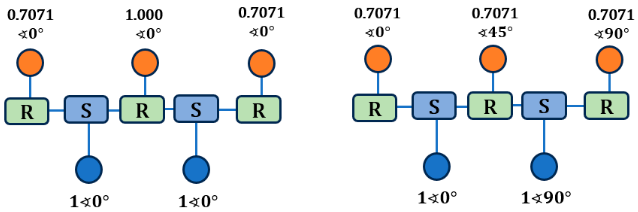

Figure 4. Phase and amplitude behavior for 2×3 CORPS networks.

Please note that there is a trade-off between the number of layers (reduction of phase shifters) and the complexity of integrating CORPS networks with spiral antenna arrays. The choice of 2×3 CORPS networks was made after a thorough study of phase behavior in networks with different numbers of layers and the scanning phase behavior of the antenna elements. Thus, a 2×3 CORPS network is useful for reducing phase shifters, and the integration challenge can be met.

2.2. Phase Behavior of a Spiral Array in Scanning

The Fermat spiral presents an interesting property in the state of the art for designing aperiodic arrays: a constant mean distance between neighboring elements [29–31]. Furthermore, the Fermat spiral presents as an advantage that the positions of the elements in the plane are calculated from simple equations, which avoids significant computational time when compared to other techniques for generating aperiodic arrays. This simplicity remains for arrays with many elements. The elements are set in the configuration of the spiral, as illustrated in Figure 5. The positions are obtained using the following coordinates [19]:

$$\rho_n = \frac{d}{d_{14}}\sqrt{n} \tag{6}$$

$$\alpha_n = n\pi\,(3 - \sqrt{5}\,) \tag{7}$$

where ρ_n is the radial distance of each antenna element; α_n is the angle of two adjacent elements; $n\pi\,(3 - \sqrt{5}\,)$ is the golden angle and $d_{14} = \sqrt{5 - 4cos(\alpha_n)}$. The equations are given in a discrete way of the Fermat spiral and can be set for a minimal distance d between antennas. The radiation pattern can be determined as expressed in [19]:

$$\vec{E}\,(\vec{r}\,) = \vec{E}_0\,(\vec{r}\,) \sum_{n=1}^{N} a_n e^{[jk(x_n sin\theta cos\phi + y_n sin\theta sin\phi + \beta_n)]} \tag{8}$$

with $\vec{E}_0(\vec{r})$ as the element pattern; $k = 2\pi/\lambda$, θ and ϕ are the elevation and azimuth angles respectively; a_n is the amplitude excitation for each antenna element and N is the number of elements for each antenna element position (x_n, y_n), which is calculated using the next expression:

$$x_n = \rho_n \cos(\alpha_n) \quad (9)$$

$$y_n = \rho_n \sin(\alpha_n) \quad (10)$$

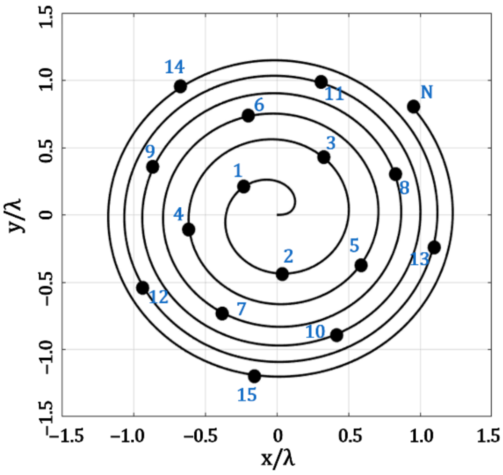

Figure 5. Fermat spiral configuration with antenna elements.

Additionally, the required phase for every antenna element (β_n) for a scanning direction given by (θ_0, ϕ_0) is obtained as:

$$\beta_n = -(x_n sin\theta_0 cos\phi_0 + y_n sin\theta_0 sin\phi_0) \quad (11)$$

The phase behavior of an aperiodic array does not exhibit the same relationship between consecutive elements. As indicated by Equation (11), the phase required by each element is defined by its respective position. Thus, aperiodic positions also generate aperiodic phases, making it difficult to obtain a linear phase slope between consecutive elements or elements with the same required phase. In this work, a distance of $d = 0.5\ \lambda$ has been chosen so that the simulation remains simple and the simplification proposal can be validated. However, it is important to note that the Fermat spiral allows suppression of grating lobes for minimum distances greater than 0.5 λ, something that a conventional array like the rectangular one does not achieve. Figure 6 shows the phases required (or the behavior of the co-phasal excitation) for a Fermat spiral array of $N = 18$ and minimal distance $d = 0.5\ \lambda$ when the main beam is scanned to $\theta_0 = 5°$ and $\theta_0 = 10°$ in the cut of $\phi = 0°$. Required phases for every element in each scanning direction are calculated using expression 11 for antenna elements, as shown in Figure 5 with $N = 18$. It can be noticed in Figure 6a that there are no elements that share the same phase required in scanning, and there is also no visible relationship between the phases of elements.

On the other hand, it can be observed that Figure 6a,b demonstrate very similar phase behavior. Thus, the phases required at $\theta_0 = 10°$ are very close to double those required at $\theta_0 = 5°$. The characteristic exhibited by elements 1, 2, and 3 is an important point. It can be observed that a phase slope very close to linear is obtained between these elements. This is maintained as one scan in directions further from $\theta_0 = 0°$. Thus, a CORPS 2×3 network could be used for the beam-forming network of these elements. Furthermore, if groups of elements in the spiral array are created such that these groups also exhibit scanning behavior similar to that exhibited by elements 1, 2, and 3, the entire array could be fed with CORPS 2×3 networks, thus simplifying the beam-forming network of the entire array.

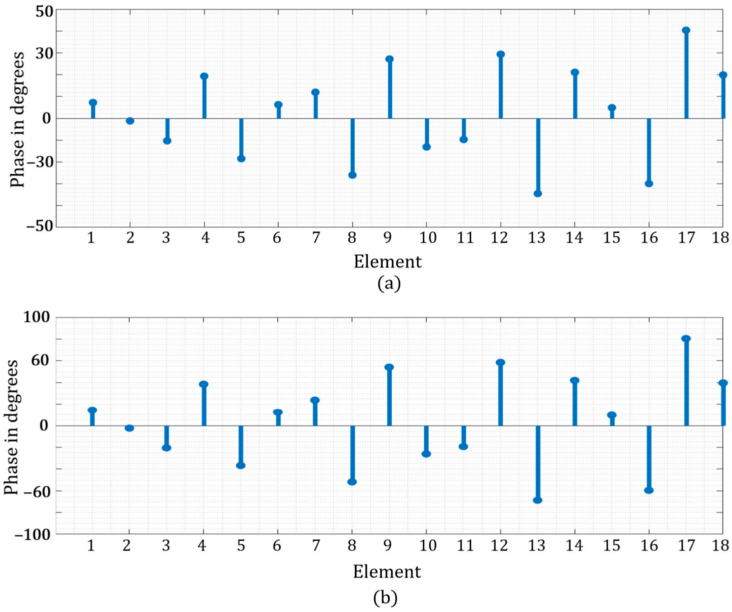

Figure 6. Phase behavior of a Fermat spiral array in the cut $\phi = 0^\circ$ at: (**a**) $\theta_0 = 5^\circ$; (**b**) $\theta_0 = 10^\circ$.

After a phase behavior analysis, groups of three elements can be formed in the array, which have the characteristic of a linear phase slope in the scan. These groups of three elements can be seen in the Figure 7. The position of elements 16 and 18 was altered to ensure that no element is left out of the groups. However, they still maintain a minimum distance of 0.5 λ. Furthermore, the elements were grouped so that they were located in the same section of the Cartesian plane, as indicated in Figure 8. The proposal to group the elements in the same section is so that they can be fed with their respective CORPS 2×3 network and that the integration of CORPS network and spiral arrays can be achieved.

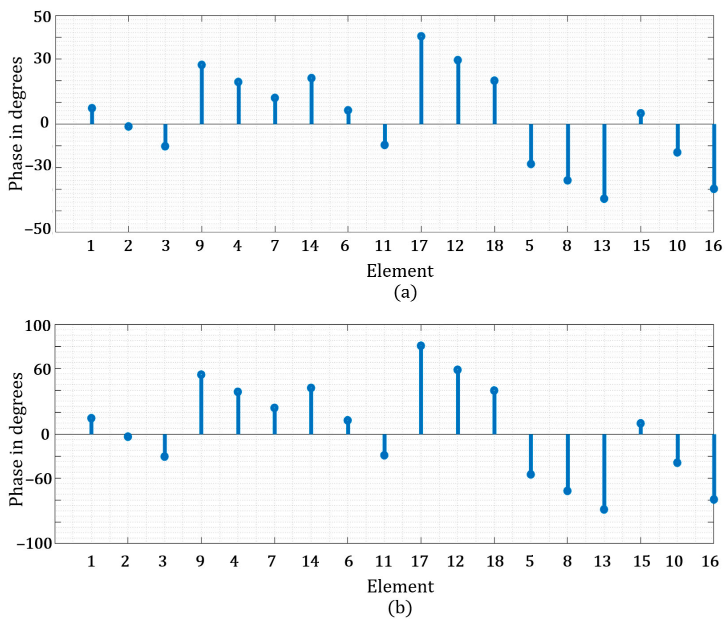

Figure 7. Phase behavior in scanning of a Fermat spiral array with groups of elements: (**a**) 5°; (**b**) 10°.

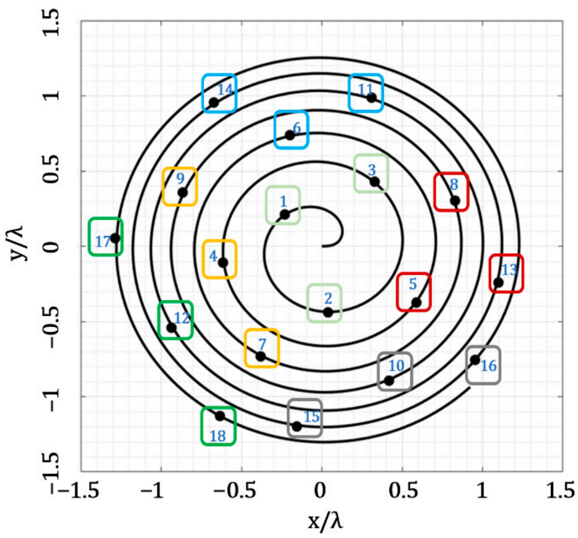

Figure 8. Groups of elements in Fermat spiral array to operate with CORPS 2×3.

Table 1 indicates the elements that belong to each CORPS 2×3 network. There are six CORPS 2×3 networks to be used for a Fermat spiral array of 18 elements. No element has been moved from its original position obtained using the Fermat spiral equations, with the exception of elements 16 and 18. Spiral array systems of a higher number of antenna elements can be grouped in sub-arrays of 2×3 CORPS networks following the described phase behavior. Therefore, the scalability of the system is not limited by the CORPS networks and is perfectly feasible.

Table 1. CORPS 2×3 networks in spiral array.

Element	CORPS 2×3	Element	CORPS 2×3	Element	CORPS 2×3
1 2 3	Network 1	14 6 11	Network 3	5 8 13	Network 5
9 4 7	Network 2	17 12 18	Network 4	15 10 16	Network 6

The integration model we are proposing uses one layer for the feeding network and another layer for the antenna array interconnected with coaxial connectors as the model shown in Figure 9. The aim is that the CORPS network outputs are located directly below the antenna elements so that coaxial connectors can be used to achieve the connection between CORPS network outputs and the antenna elements. This approach will allow us to allocate more space for design of the feeding network and avoid unwanted radiation in the radiation pattern of the spiral array system.

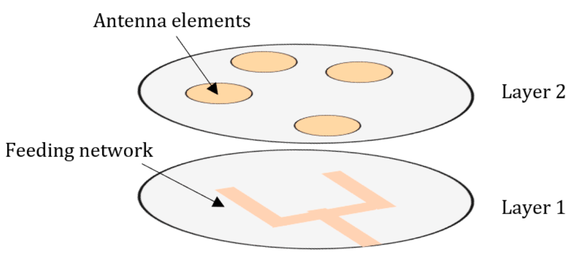

Figure 9. Proposal of integration model for spiral array with CORPS networks.

The characteristics of the Fermat spiral cause the phase slope to be not exactly linear in scanning. However, there is only a slight difference of a few degrees between the phase required for each central element in the array and the phase obtained with a 2×3 CORPS network. The fact that only the central element presents a difference is due to the characteristic of CORPS 2×3 networks. This difference is shown in Tables 2 and 3 for scanning at θ_0 = 5° and θ_0 = 22° (in the cut of ϕ = 0°), respectively. The maximum difference is approximately 3° at the maximum scan angle (θ_0 = 22°).

Table 2. Differences between required phases and phases obtained by CORPS 2×3 networks in θ_0 = 5°.

Element	Required Phase (°)	CORPS Phase (°)	Difference	Element	Required Phase (°)	CORPS Phase (°)	Difference
1	7.2196	7.2196	0	17	40.3433	40.3433	0
2	−1.2111	−1.5500	0.3389	12	29.3523	30.1131	0.7608
3	−10.3196	−10.3196	0	18	19.8830	19.8830	0
9	27.1560	27.1560	0	5	−18.4774	−18.477	0
4	19.2869	19.5489	0.2620	8	−26.0170	−26.481	0.4644
7	11.9417	11.9417	0	13	−34.4854	−34.485	0
14	21.0753	21.0753	0	15	4.8727	4.8727	0
6	6.2281	5.6775	0.5506	10	−13.1246	−12.527	0.5977
11	−9.7203	−9.7203	0	16	−29.9265	−29.926	0

Table 3. Differences between required phases and phases obtained by CORPS 2×3 networks in θ_0 = 22°.

Element	Required Phase (°)	CORPS Phase (°)	Difference	Element	Required Phase (°)	CORPS Phase (°)	Difference
1	31.0309	31.0309	0	17	173.4009	173.4009	0
2	−5.2055	−6.6620	1.4565	12	126.1600	129.4304	3.2704
3	−44.3549	−44.3549	0	18	85.4598	85.4598	0
9	116.7199	116.7199	0	5	−79.4181	−79.4181	0
4	82.8974	84.0235	1.126	8	−111.824	−113.820	1.9959
7	51.3271	51.3271	0	13	−148.223	−148.2235	0
14	90.5844	90.5844	0	15	20.9435	20.9435	0
6	26.7694	24.4027	2.3667	10	−56.4113	−53.8422	2.5691
11	−41.7791	−41.7791	0	16	−128.628	−128.628	0

The array factor has been calculated for both the required and CORPS phases and is shown in Figure 10. It can be noticed that there is no significant difference in array performance when using the phases of CORPS 2×3 networks, so this technique can be used properly to simplify the feed network of a Fermat spiral array.

The spiral configuration allows the suppression of grating lobes for distances between elements greater than 0.5 λ. Table 4 shows the difference between required phases and CORPS phases for the case with minimum distance of 1.0 λ and θ_0 = 10°. The maximum difference is approximately 3°. Figure 11 illustrates the array factor of this design case for θ_0 = 5° and θ_0 = 10° using uniform distribution. It can be noted that there is no significant variation between the patterns with required phases and using the CORPS phases. Also note that there are no grating lobes in the radiation pattern. This is due to the use of an aperiodic structure such as the spiral.

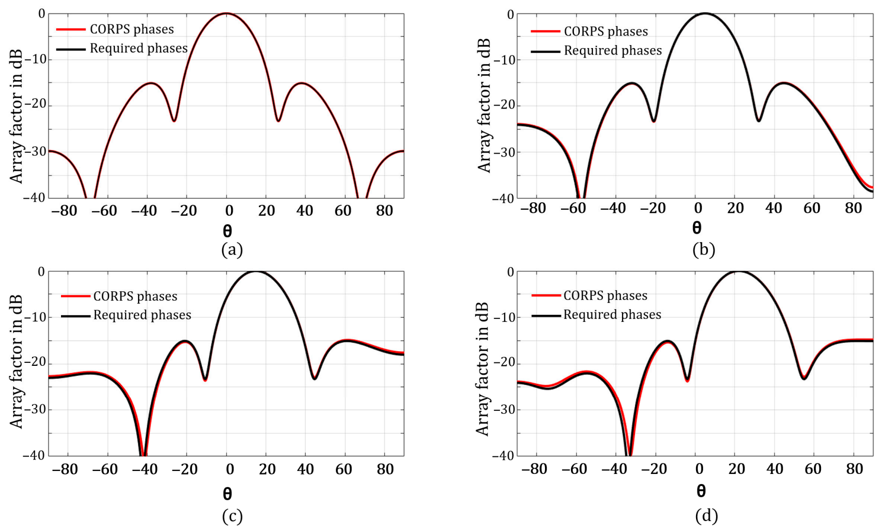

Figure 10. Comparison of array factor using required and CORPS phases, (**a**) θ_0 = 0°; (**b**) θ_0 = 5°; (**c**) θ_0 = 15°; (**d**) θ_0 = 22°.

Table 4. Differences between required phases and phases obtained by CORPS in θ_0 = 10° with $d_{min} = 1.0\ \lambda$.

Element	Required Phase (°)	CORPS Phase (°)	Difference	Element	Required Phase (°)	CORPS Phase (°)	Difference
1	28.7686	28.7686	0	17	160.7593	160.7593	0
2	−4.8260	−6.1764	1.3504	12	116.9625	119.9943	3.0318
3	−41.1213	−41.1213	0	18	79.2294	79.2294	0
9	108.2106	108.2106	0	5	−73.6282	−73.6282	0
4	76.8539	77.8979	1.0440	8	−103.6721	−105.5225	1.8504
7	47.5852	47.5852	0	13	−137.4168	−137.4168	0
14	83.9804	83.9804	0	15	19.4166	19.4166	0
6	24.8178	22.6236	2.1942	10	−52.2987	−49.9169	2.3818
11	−38.7333	−38.7333	0	16	−119.2505	−119.2505	0

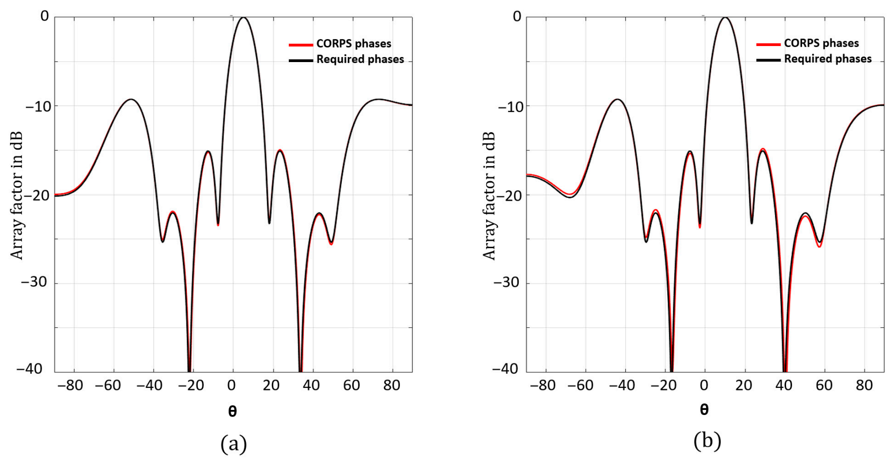

Figure 11. Comparison of array factor using required and CORPS phases with $d_{min} = 1.0\lambda$, (**a**) θ_0 = 5°; (**b**) θ_0 = 10°.

2.3. Amplitude Distribution for SLL Minimization

The aperiodic characteristic of a Fermat spiral array eliminates grating lobes and also allows for low sidelobe levels. However, these levels may not be maintained in beam scanning, so non-uniform distribution techniques can be used with techniques focused on maintaining feed network simplification. We will try to illustrate several possibilities to generate the excitation distribution. Furthermore, the possibility of using CORPS amplitudes, that is, those obtained directly from the output of each CORPS 2×3 network, is interesting. This way, no compensation is required to generate the necessary amplitude distribution.

2.3.1. Raised Cosine Excitation

The raised cosine excitation is generally used for lineal arrays [32]. However, it is used in this work to calculate the amplitudes for a spiral array (bidimensional). The application of a raised cosine excitation can be given by using the next expression [33]:

$$I_n = \frac{1 + \cos\left(\frac{d_n cos^{-1}(2a-1)}{0.5L}\right)}{2} \quad n = 1, 2, 3 \ldots, N \tag{12}$$

where d_n is the separation from the system center to the nth element, L is the length of the array longitude in x and a is considered a constant value. Furthermore, I_n is set to be in the interval of a < I_n < 1.

Figure 12 shows the way that the rings (areas) were set so that the elements within a ring have a value of assigned amplitude excitation. The index n indicates the amplitude value for each element (considering d_n). Then, d_n is determined by using the rings n and $n-1$. Finally, the value of L is determined as the distance value considering the center to the furthest element. The proposed raised cosine technique allows for the use of only four amplitude values instead of 18. This allows for a simplification of the feed network for a spiral array.

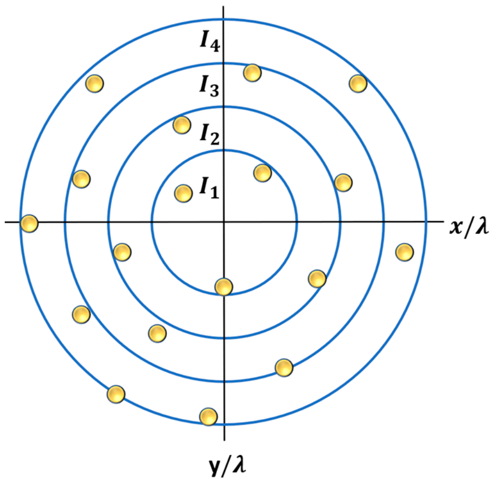

Figure 12. Raised cosine excitation for the Fermat spiral array.

2.3.2. Optimization of Amplitude Excitations

This design technique contemplates the use of GA. The technique of GA has been applied successfully in the design of different antenna systems [34]. The optimization procedure of GA follows the steps explained in [35]. The design variables (amplitudes excitations) are coded in a set of real numbers, $I = [I_1, I_2, I_3, I_4, \ldots, I_N]$, which can be set in the range of values [0, 1]. The design problem consists of determining the amplitude excitations that minimize the SLL value. The design problem can be described as the minimization of the next design objective:

$$OF = SLL_{max}(AF(\theta, \phi)) \tag{13}$$

where SLL_{max} is the maximum value of SLL obtained for all cuts of ϕ = [0, 2π] and $\theta = [-\frac{\pi}{2}, \frac{\pi}{2}]$. It was considered in our design case the evaluation of the radiation pattern for each cut of ϕ, in steps of 10°. This SLL_{max} is only evaluated in all cuts of ϕ for scanning. As shown in Figure 13, there is an amplitude excitation considered for each element with this method.

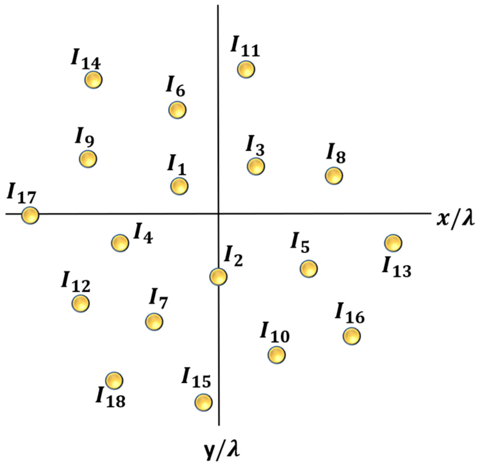

Figure 13. Amplitude excitations using genetic algorithms in the array geometry.

2.3.3. CORPS Amplitudes

A CORPS 2×3 network causes an attenuation in the amplitude of the middle output if a difference of phases exists in the input signals, and this attenuation increases as the difference approaches 180°. Thus, it is necessary to compensate the values using a variable amplifier at the output port of each recombination node. The compensation depends on the amplitude excitation required in each antenna element obtained with raised cosine or optimization [28]. Furthermore, the phases required by the elements in beam scanning change so that amplitudes required at θ_0 = 0° are not the same as those required at θ_0 = 22°. Thus, a compensation is needed in each direction in order to maintain the amplitude distribution required. However, we could consider the case of taking the amplitude values obtained directly of the CORPS 2×3 networks. Thus, it would not be necessary to include variable amplifiers in the feeding network, allowing the maximum simplification of the antenna system.

3. Results and Discussion

The proposed simplification case using CORPS 2×3 networks was implemented using the amplitude distributions described in the previous section to evaluate the SLL reduction. The results of these cases are illustrated in this section, and a comparative analysis has been made among the different techniques. All the design cases considered a value of N = 18 antenna elements and a minimal distance of d = 0.5 λ.

3.1. Electromagnetic Characterization

The proposed design cases for the Fermat spiral with CORPS 2×3 networks were electromagnetically characterized by using CST Microwave Studio. This was made to analyze the performance of the proposed design cases, considering the effects of mutual coupling among the elements and the effect of the radiation pattern of the antenna element. A circular patch for a center frequency of 6 GHz was considered as the antenna element using an Arlon 25 N substrate with the following characteristics: substrate thickness h = 1.54 mm, epsilon = 3.38, and tangential losses = 0.0025. The design in CST is showed in Figure 14. The values of r and p' are 6.82 and 2.36, respectively.

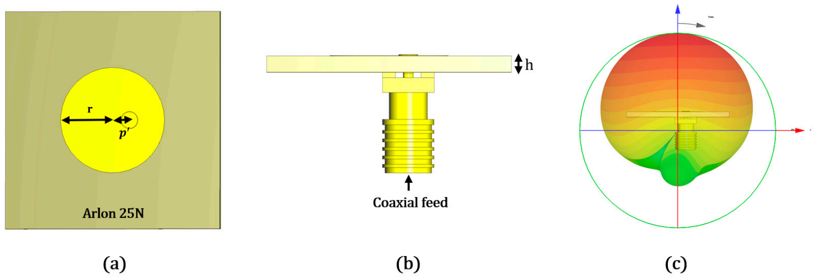

Figure 14. Design of CST of the circular antenna for a center frequency of 6 GHz: (**a**) top view; (**b**) side view; (**c**) radiation pattern.

Figure 15 illustrates the design of the antenna array set in CST using 18 elements in the Fermat spiral configuration. The dimensions of this array design were set to have a value of r = 73 mm. Different values of phase and amplitude are chosen to feed the antenna elements, depending on the beam-scanning direction and the amplitude distribution. The phase values are the obtained by CORPS 2×3 networks, such as the CORPS phases in Tables 2 and 3. Next, the different distribution techniques are presented and assessed to set certain criteria for antenna designers.

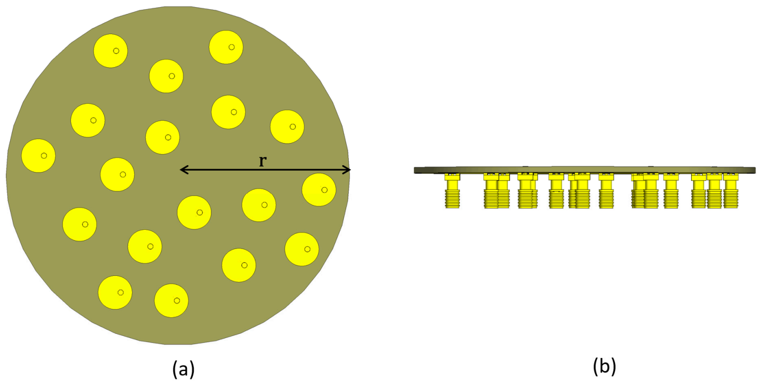

Figure 15. Design of spiral array antenna in CST for CORPS networks: (**a**) top view; (**b**) side view.

3.2. Raised Cosine Distribution

Each antenna element is fed using a value of amplitude excitation depending on its position in the plane (ring). This implementation requires only four amplitude values for the whole antenna system. This is useful for simplifying the feeding network of the array system. Furthermore, the value of a was set to be 0.30 in Equation (12). The assessment of SLL behavior considers the cuts of ϕ = [0, 2π] for $\theta_0 = 0°$ for the case of natural response. The cut of ϕ = 0° was evaluated for the case of scanning in the range of $\theta_0 = [-22°,\ 22°]$. Figure 16 shows the radiation pattern obtained for the natural response of the array system ($\theta_0 = 0°$). In this pattern, the highest SLL is −16.1 dB for the cut of ϕ = 120° and the lowest SLL is −27.9 dB for ϕ = 170°. On the other hand, Figure 17 illustrates the radiation pattern considering the case of scanning in directions at $\theta_0 = 5°, 10°, 15°$, and 22° with ϕ = 0°. The scanning SLL performance is maintained below −23.1 dB through the entire scanning range of $\theta_0 = [-22°, 22°]$. Please note that the values of SLL in natural response and scanning can be different. This case of raised cosine distribution could be useful to antenna designers because only four amplitude levels are used throughout the scanning range.

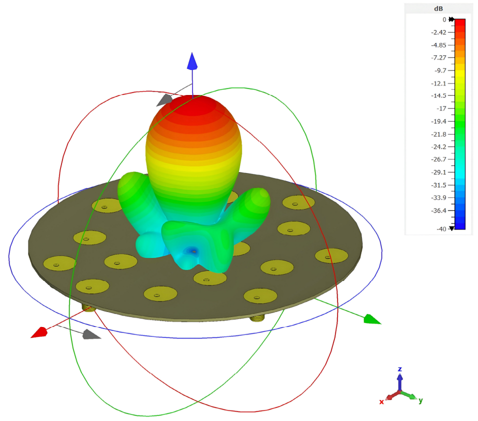

Figure 16. 3D radiation pattern (CST) for the design case using raised cosine distribution natural response of the array system $\left(\theta_0 = 0^{\circ}\right)$.

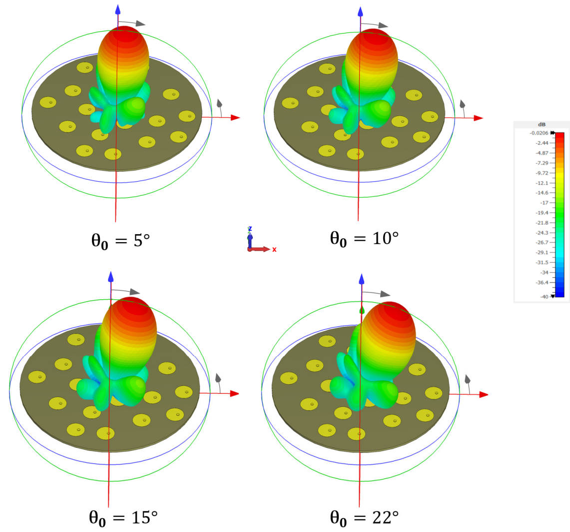

Figure 17. 3D radiation pattern (scanning) CST for the case using raised cosine distribution.

3.3. Amplitude Distribution Using Evolutionary Optimization

The optimization parameters for this design case were set considering the recommendations set in the literature and our experience in the design of antenna arrays [34,36]. A crossover probability of 1.0 was used and the mutation probability was set as 0.1. The optimization algorithm was run in a number of iterations of 1000 and set to reach convergence. The population size was set at a value of twice the number of the decision variables considered in the design problem. All the design cases considered a value of N = 18 antenna elements and a minimal distance of d = 0.5 λ. The evaluation of SLL performance considered cuts of ϕ = [0, 2π] for $\theta_0 = 0^{\circ}$ for the case of natural response. The cut of ϕ = 0° was evaluated for the case of scanning in the range of $\theta_0 = [-22^{\circ}, 22^{\circ}]$.

Figure 18 show the results of the radiation pattern generated by using the optimized amplitudes for $\theta_0 = 0^{\circ}$ or natural response (without scanning). The optimization of the amplitudes provides the best SLL response (−22.1 dB) in the cut of ϕ = 30° and the worst case of SLL (−19.4 dB) in the cut of ϕ = 130°. On the other hand, Figure 19 illustrates the response of the radiation pattern considering the scanning direction at $\theta_0 = 5^{\circ}$, 10°, 15°, 22° with ϕ = 0°, using the amplitudes optimization. The SLL performance is maintained below −19.6 dB, considering beam-scanning in all directions of the range of $\theta_0 = [-22^{\circ}, 22^{\circ}]$. The values of SLL in natural response and scanning can be different. Please note that this performance is reached by using one amplitude level by each antenna element.

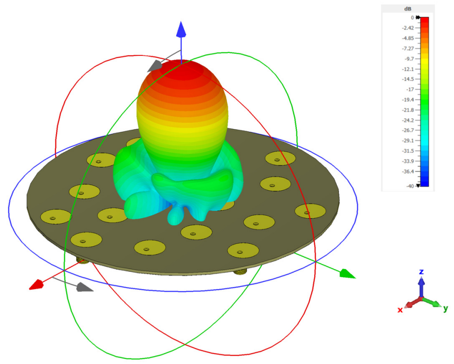

Figure 18. 3D radiation pattern (CST) for the design case using amplitudes optimization: natural response of the array system ($\theta_0 = 0°$).

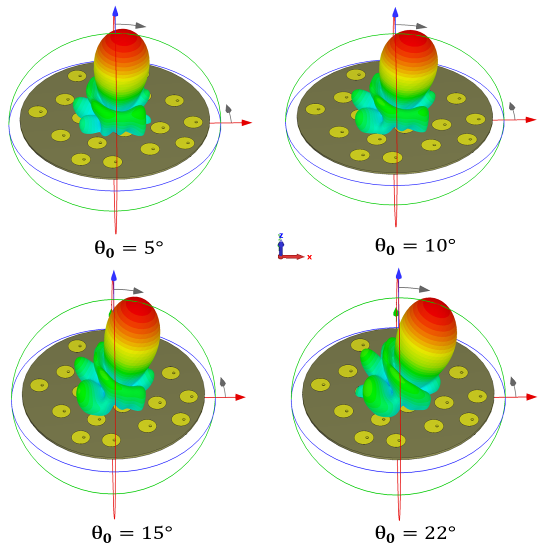

Figure 19. 3D radiation pattern (scanning) in CST for the case using amplitudes optimization.

3.4. Amplitude Distribution Using the CORPS Feeding Networks

We could take advantage of the simplification of the feeding network and take the amplitude levels generated by the feeding network system. The evaluation of SLL performance considered cuts of ϕ = [0, 2π] for $\theta_0 = 0°$ for the case of natural response. The cut of ϕ = 0° was evaluated for the case of scanning in the range of $\theta_0 = [-22°, 22°]$.

Figure 20 shows the radiation pattern using the amplitude values of the CORPS networks for the case of natural response $(\theta_0 = 0^{\circ})$. The best value of SLL (−18.5 dB) is obtained in the cut of ϕ = 90° and the worst case (−15.5 dB) is generated in the cut of ϕ = 120°. The scanning performance is illustrated in Figure 21, considering the direction at $\theta_0 = 5°, 10°, 15°, 22°$ with ϕ = 0°. As illustrated in this figure, a value of SLL= −13.8 dB $(\theta_0 = 22^{\circ})$ remains, with a minimum value of SLL = −17.3 dB at $\theta_0 = 0^{\circ}$. Please note that this SLL performance is obtained without using amplitude excitations, just taking the amplitude levels generated by the feeding network.

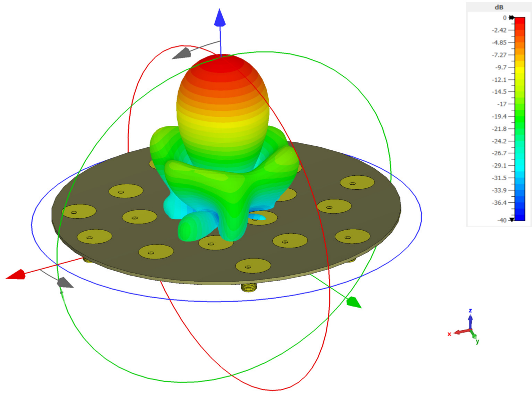

Figure 20. 3D radiation pattern (CST) for the design case using amplitude levels of feeding networks: natural response of the array system.

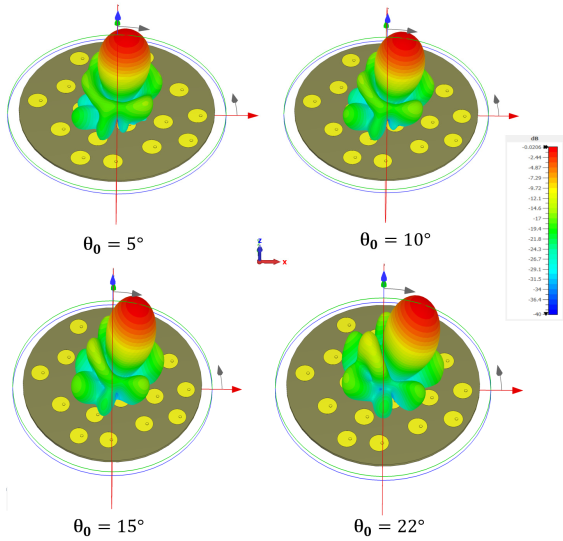

Figure 21. 3D radiation pattern (scanning) in CST for the design case, using amplitude levels of feeding network.

3.5. Uniform Amplitude Distribution

The last amplitude distribution case to be presented is the uniform amplitude case. Figures 22 and 23 show the radiation pattern obtained for the natural response of the array system $(\theta_0 = 0^{\circ})$ and scanning, respectively. The evaluation of SLL performance considered cuts of $\phi = [0, 2\pi]$ for $\theta_0 = 0^{\circ}$ for the case of natural response. The cut of $\phi = 0^{\circ}$ was evaluated for the case of scanning in the range of $\theta_0 = [-22^{\circ}, 22^{\circ}]$.

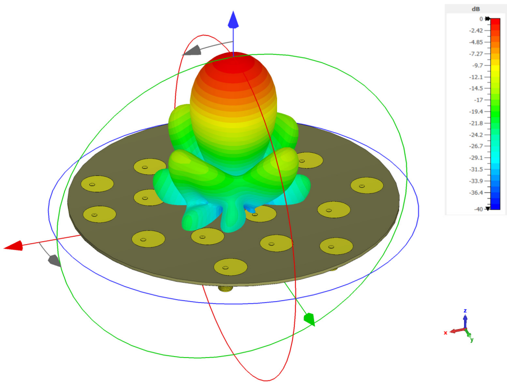

Figure 22. 3D radiation pattern (CST) using uniform amplitude distribution: natural response of the array system $(\theta_0 = 0^{\circ})$.

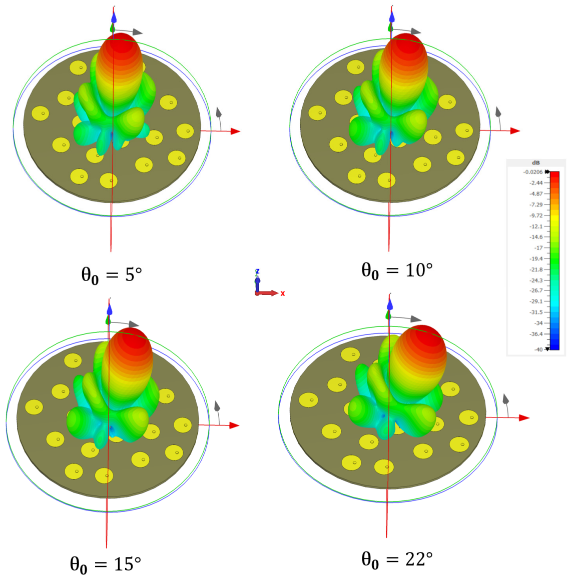

Figure 23. 3D radiation pattern (scanning) in CST using uniform amplitude distribution.

As illustrated in Figure 22, the best SLL (−20.5 dB) is obtained for ϕ = 70° and the worst case of −13.8 dB is generated in the cut of ϕ = 120°.

This case could be of interest to set levels of uniform amplitude in the antenna elements of the array system. However, the uniform excitation requires one amplitude level by each antenna element for this particular design of spiral array. This is because the amplitudes of the feeding network outputs are non-uniform. So, we need to compensate for these amplitudes differences if the uniform distribution is desired. The scanning performance is illustrated in Figure 23, considering the direction of the main beam at $\theta_0 = 5°, 10°, 15°, 22°$ with ϕ = 0°. A value of SLL = −15.7 dB remains in the scanning performance.

3.6. Design of Array Antenna in CST with $d_{min} = 1.0\lambda$

Figure 24 illustrates the design of the antenna array in CST using $d_{\text{min}} = 1.0\lambda$. The dimensions of this array design were set to have a value of r = 138 mm. The phases values are obtained using CORPS 2×3 networks such as the CORPS phases in Table 4. A uniform distribution was used for this case, and the patterns were obtained for $\theta_0 = 5°$ and $\theta_0 = 10°$, as shown in Figure 25.

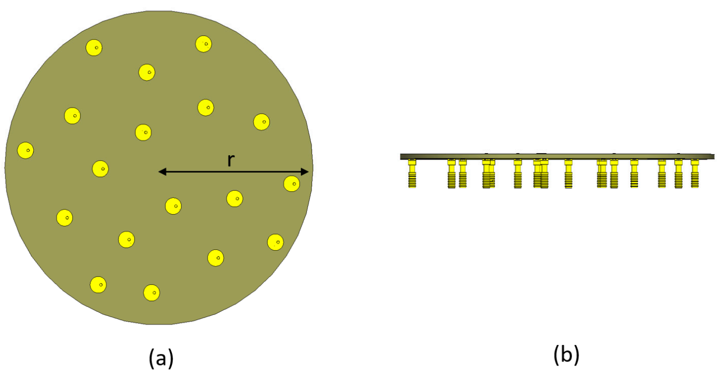

Figure 24. Design of spiral array antenna in CST with $d_{\text{min}} = 1.0\lambda$: (**a**) top view; (**b**) side view.

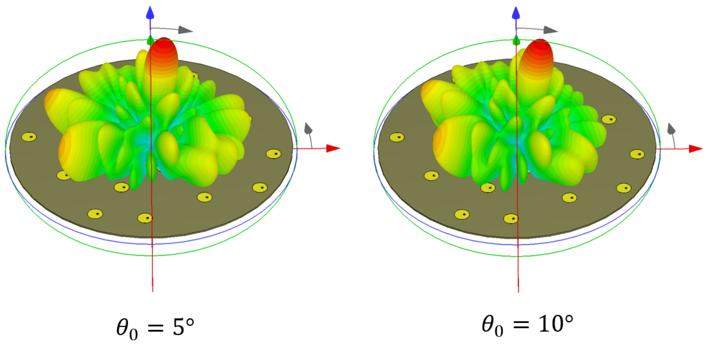

Figure 25. 3D radiation pattern (scanning) in CST with $d_{min} = 1.0\lambda$.

The SLL in the cut of ϕ = 0° is −12.0 dB for $\theta_0 = 5°$ and −10.9 dB for $\theta_0 = 10°$. Please note that no amplitude distribution technique is being used to decrease the SLL. This is with the aim of simplifying the presentation of results for this design case ($d_{min} = 1.0\lambda$).

3.7. Comparative Assesment of the Amplitude Distributions

There are certain design criteria among the set amplitude distributions. These design tradeoffs can be observed using the numbers in Tables 5 and 6. These tables illustrate a comparative analysis of the SLL performance in $\theta_0 = 0°$. The comparison made in these tables is between cases with $d_{min} = 0.5\lambda$. It can be noted that all design cases present an SLL less than −15 dB at each cut of ϕ, with the exception of ϕ = 110°, 120°, and 130° for the uniform distribution case. The raised cosine is the distribution that reaches the lowest values in most cuts with respect to the other cases. Amplitudes optimization presents the lowest values after the raised cosine distribution, with the tradeoff that one amplitude level is needed per antenna element. The raised cosine distribution presents lower SLL values compared to the amplitude's optimization in several cuts of the radiation pattern. This is presented in the cuts of ϕ = [10°, 40°, 50°, 80°, 90°, 140°, 150°, 160°, 170°, 180°]. Furthermore, it presents a difference of less than 1 dB in the cuts of ϕ = 20°, 30°, and 140°. Another important case is the behavior of the CORPS amplitude distribution. It can be observed that lower values are presented in most of the cuts with respect to the uniform distribution (with the exception of the cuts ϕ = [60°, 70°, 80°, 90°, 140°, 150°, 170°]). Furthermore, it has a difference of less than 1 dB in ϕ = 70°, 90°, and 140°. The performance of CORPS amplitudes distribution is very interesting, considering that the values of *SLL* reached in this case are obtained directly from the outputs of the CORPS 2×3 networks.

Table 5. Values obtained by the electromagnetic characterization (CST) of amplitude distribution cases, $\theta_0 = 0°$.

Design Case	**SLL (dB) Considering Values of ϕ**								
	10°	**20°**	**30°**	**40°**	**50°**	**60°**	**70°**	**80°**	**90°**
Raised cosine	−21.6	−21.1	−21.5	−22.2	−22.9	−22.7	−22.3	−22.3	−20.5
Amplitude optimization	−21.4	−21.8	−22.1	−20.7	−19.9	−19.7	−19.6	−20.0	−20.5
CORPS amplitude	−16.8	−16.7	−16.9	−16.9	−16.9	−17.1	−17.6	−18.2	−18.5
Uniform amplitude	−15.7	−15.3	−15.6	−16.2	−17.2	−18.9	−20.5	−20.5	−18.8

Table 6. Values obtained by the electromagnetic characterization (CST) of amplitude distribution cases, $\theta_0 = 0°$. Continuation.

Design Case	**SLL (dB) Considering Values of ϕ**								
	100°	**110°**	**120°**	**130°**	**140°**	**150°**	**160°**	**170°**	**180°**
Raised cosine	−17.8	−16.3	−16.1	−17.4	−20.8	−26.0	−24.8	−27.9	−24.3
Amplitude optimization	−20.7	−20.2	−19.4	−19.4	−20.9	−21.1	−21.0	−20.8	−20.8
CORPS amplitude	−17.4	−16.2	−15.5	−15.6	−16.8	−18.0	−18.36	−17.8	−17.3
Uniform amplitude	−16.3	−14.4	−13.8	−14.7	−17.0	−19.6	−20.2	−18.6	−16.7

Table 7 shows a comparative analysis of the proposed techniques considering beam scanning. It can be noted that all amplitude distributions achieve a performance of SLL less than −15 dB in all scanning ranges, with the exception of CORPS amplitudes in the direction of $\theta_0 = 22°$. These levels are the best SLL obtained. The CORPS amplitudes distribution is again a very interesting case, as it maintains a SLL below −15 dB up to $\theta_0 = 15°$. The difference of SLL in the maximum scanning angle is approximately 2 dB with respect to uniform amplitude case. So, this case could be considered to achieve the maximum simplification of the feeding network.

Table 7. Comparative analysis of amplitude distribution techniques considering beam scanning (results in CST considering the best values of SLL).

Design Case	**SLL in dB for Each Value of θ_0**				
	0°	**5°**	**10°**	**15°**	**22°**
Raised cosine	−24.3	−24.0	−23.8	−23.6	−23.1
Amplitude optimization	−20.8	−20.5	−20.5	−20.4	−19.6
CORPS amplitude	−17.3	−16.7	−16.2	−15.5	−13.8
Uniform amplitude	−16.7	−16.4	−16.3	−16.3	−15.7

Furthermore, Table 8 shows the gain behavior considering each excitation technique in beam scanning. As illustrated, the gain behavior is very similar for all the amplitude distributions. Uniform amplitude presents the highest gain, followed by CORPS amplitudes. The techniques of amplitudes optimization and raised cosine required to give a little gain to provide the given SLL value. Please note that these gain values do not include losses due to elements in the feeding network, such as attenuators and those caused by the CORPS networks.

Table 8. Gain behavior using CST electromagnetic solver considering beam scanning.

Design Case	**Gain in dBi for Each Value of θ_0**				
	0°	**5°**	**10°**	**15°**	**22°**
Raised cosine	18.05	18.02	17.97	17.88	17.72
Amplitude optimization	17.98	17.94	17.86	17.77	17.59
CORPS amplitude	18.40	18.35	18.31	18.22	17.97
Uniform amplitude	18.46	18.41	18.34	18.25	18.09

Finally, Figure 26 shows the reflection coefficients of each antenna element in beam scanning. It can be noted that in 6 GHz all antenna elements have a reflection coefficient less than −10 dB, which indicates adequate behavior for the antenna system. The simulations made in CST validated the technique proposed for simplifying the feeding network in a Fermat spiral antenna array.

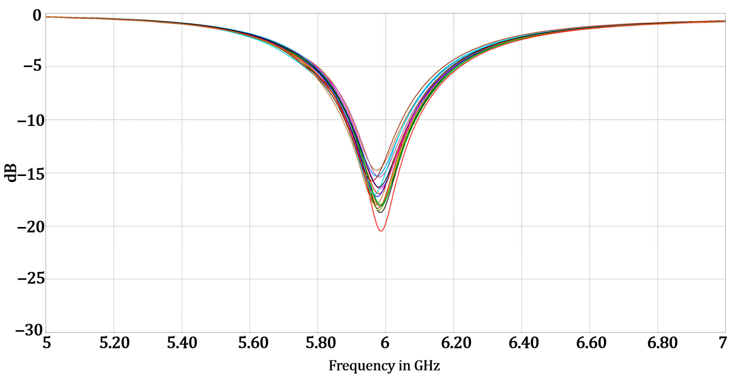

Figure 26. Behavior of the reflection coefficient versus frequency for the design of Fermat spiral antenna array with $d_{min} = 0.5\lambda$.

We have tried to make a comparison of the techniques used to reduce SLL, without seeking to show that one is the best distribution for all scenarios. We think that each technique presents a design compromise, where, indeed, the raised cosine presents one of the best performances in SLL. However, the distribution used, taking amplitudes directly from the CORPS network outputs, helps to simplify the antenna system. For this reason, we aim to present tables for comparison.

4. Conclusions

This paper presented a novel design technique using beam-forming networks based on CORPS to achieve the simplification of the feed network of Fermat spiral antenna arrays. The setting of subarrays was achieved through the study of the behavior of phases of each antenna element in scanning. This design, which considers the geometry of the Fermat spiral, uses different methods for SLL reduction. The electromagnetic simulation results illustrated that all design cases presented an SLL less than -15 dB at each cut of ϕ, with exception of ϕ = 110°, 120°, and 130° for the uniform distribution case. The raised cosine demonstrated the lowest values in most cuts with respect to the other cases. Amplitudes optimization presented the lowest values after the raised cosine distribution, with the tradeoff that one amplitude level is needed per antenna element. The raised cosine distribution presented lower *SLL* values compared to the amplitude's optimization in several cuts of the radiation pattern. This was presented in the cuts of ϕ = [10°, 40°, 50°, 80°, 90°, 140°, 150°, 160°, 170°, 180°]. Furthermore, it presented a difference of less than 1 dB in the cuts of ϕ = 70°, 90°, and 140°. The performance of CORPS amplitudes distribution is very important, considering that the values of SLL reached in this case are obtained directly of the outputs of the CORPS 2×3 networks. Furthermore, all amplitude distributions achieved a performance of SLL less than -15 dB in all scanning ranges, with the exception of CORPS amplitudes in the direction of $\theta_0 = 22°$. Raised cosine reached the lowest values in scanning, followed by amplitudes optimization. The CORPS amplitudes distribution can be considered a useful case to achieve the maximum simplification of the feeding network, as it maintains an SLL below -15 dB up to $\theta_0 = 15°$. Furthermore, a design case was presented to show the absence of grating lobes in spiral arrays with $d_{min} = 1.0\lambda$ and to illustrate the use of CORPS 2×3 networks with spiral arrays using distances greater than 0.5λ. Choosing CORPS 2×3 networks would allow CORPS integration with spiral arrays by proposing a section for the feed network and a section for the antenna array, in order to avoid crossings and reduce unwanted radiation in the radiation pattern of the antenna system.

Author Contributions: Conceptualization, M.A.P. and K.E.; methodology, K.E. and D.H.C.; software, K.E. and D.H.C.; validation, A.R. and M.A.P.; formal analysis, K.E. and M.A.P.; investigation, A.R. and L.A.G.; resources, M.A.P. and A.R.; data curation, K.E. and L.A.G.; writing—original draft preparation, M.A.P. and K.E.; writing—review and editing, M.A.P. and K.E.; visualization, D.H.C. and L.A.G.; super vision, M.A.P.; project administration, M.A.P. and A.R.; funding acquisition, M.A.P. and L.A.G. All authors have read and agreed to the published version of the manuscript.

Funding: This paper has been supported by the Secretaria de Ciencia, Humanidades, Tecnología e Innovación México under grant PEE-2025-G-266.

Data Availability Statement: The original contributions presented in this study are included in the article. Further inquiries can be directed to the corresponding author.

Conflicts of Interest: The authors declare no conflicts of interest.

Abbreviations

The following abbreviations are used in this manuscript:

CORPS	Coherently Radiating Periodic Structures
SLL	Side Lobe Level
GA	Genetic Algorithms
CST	Computer Simulation Technology

References

1. Lai, Q.; Gao, C.; Peng, T.; Liu, Z.; Wang, X.; Wu, H.; Ma, J. A digital beam-forming multiple-beam reflector antenna subsystem for GEO communication satellites. In *Proceedings of the 2016 46th European Microwave Conference (EuMC), London, UK, 4–6 October 2016*; IEEE: New York, NY, USA, 2016; pp. 866–869. [CrossRef]
2. Han, G.; Du, B.; Wu, W.; Yang, B. A Novel Hybrid Phased Array Antenna for Satellite Communication on-the-Move in Ku-band. *IEEE Trans. Antennas Propag.* **2015**, *63*, 1375–1383. [CrossRef]
3. Syrytsin, I.; Zhang, S.; Pedersen, G.F.; Morris, A.S. Compact Quad-Mode Planar Phased Array with Wideband for 5G Mobile Terminals. *IEEE Trans. Antennas Propag.* **2018**, *66*, 4648–4657. [CrossRef]
4. Shen, X.; Liu, Y.; Zhao, L.; Huang, G.-L.; Shi, X.; Huang, Q. A Miniaturized Microstrip Antenna Array at 5G Millimeter-Wave Band. *IEEE Antennas Wirel. Propag. Lett.* **2019**, *18*, 1671–1675. [CrossRef]
5. Won, H.; Hong, Y.-K.; Li, L.; Awasthi, A.; Nickerson, N.; Bryant, B.; Choi, M.; Yan, S.; Taylor, D.; O'NEill, C.; et al. VHF/UHF Open-Sleeve Dipole Antenna Array for Airborne Ice Sounding and Imaging Radar. *IEEE Antennas Wirel. Propag. Lett.* **2021**, *20*, 883–887. [CrossRef]
6. Yang, X.; Liu, X. Design of a Wide-Beam Microstrip Array Antenna for Automotive Radar Application. *IEEE Access* **2021**, *9*, 142340–142347. [CrossRef]
7. Yoo, S.; Milyakh, Y.; Kim, H.; Hong, C.; Choo, H. Patch Array Antenna Using a Dual Coupled Feeding Structure for 79 GHz Automotive Radar Applications. *IEEE Antennas Wirel. Propag. Lett.* **2020**, *19*, 676–679. [CrossRef]
8. Mar, J.; Liu, C.-C.; Basnet, M.B. Ship-Borne Phased Array Radar Using GA Based Adaptive α–β–γ Filter for Beamforming Compensation and Air Target Tracking. *Int. J. Antennas Propag.* **2015**, *2015*, 1–16. [CrossRef]
9. Canabal, A.; Jedlicka, R.P.; Pino, A.G. Multifunctional phased array antenna design for satellite tracking. *Acta Astronaut.* **2005**, *57*, 887–900. [CrossRef]
10. Raghu, N.; Manjunatha, K.N.; Kiran, B. Tracking of satellites by using Phased Array Antenna. In *Proceedings of the 2014 International Conference on Electronics and Communication Systems (ICECS), Coimbatore, India, 13–14 February 2014*; IEEE: New York, NY, USA, 2014; pp. 1–6. [CrossRef]
11. Heidari, H.R.; Rezaei, P.; Kiani, S.; Taherinezhad, M. A monopulse array antenna based on SIW with circular polarization for using in tracking systems. *AEU—Int. J. Electron. Commun.* **2023**, *162*, 154563. [CrossRef]
12. Capelli-Mouvand, T.; Ghiotto, A.; Cathelin, P.; Deltimple, N. 5G Millimeter Wave Active Phased-Array Antenna Active Load Pulling Evaluation on Power Amplifiers. In *Proceedings of the 2021 15th European Conference on Antennas and Propagation (EuCAP), Dusseldorf, Germany, 22–26 March 2021*; IEEE: New York, NY, USA, 2021; pp. 1–5. [CrossRef]

13. Gutierrez, A.R.; Reyna, A.; Balderas, L.I.; Panduro, M.A.; Mendez, A.L. Nonuniform Antenna Array with Nonsymmetric Feeding Network for 5G Applications. *IEEE Antennas Wirel. Propag. Lett.* **2022**, *21*, 346–350. [CrossRef]
14. Reyna, A.; Panduro, M.A.; del Rio-Bocio, C. On the Design of Concentric Ring Arrays for Isoflux Radiation in MEO Satellites Based on PSO. *Prog. Electromagn. Res. M* **2011**, *20*, 243–255. [CrossRef]
15. Bataineh, M.H.; Ababneh, J.I. Synthesis of Aperiodic Linear Phased Antenna Arrays Using Particle Swarm Optimization. *Electromagnetics* **2006**, *26*, 531–541. [CrossRef]
16. El-makadema, A.; Rashid, L.; Brown, A.K. Geometry Design Optimization of Large-Scale Broadband Antenna Array Systems. *IEEE Trans. Antennas Propag.* **2014**, *62*, 1673–1680. [CrossRef]
17. Buttazzoni, G.; Babich, F.; Pastore, S.; Vatta, F.; Comisso, M. Gaussian Approach for the Synthesis of Periodic and Aperiodic Antenna Arrays: Method Review and Design Guidelines. *Sensors* **2021**, *21*, 2343. [CrossRef]
18. Viganó, M.C.; Toso, G.; Caille, G.; Mangenot, C.; Lager, I.E. Sunflower Array Antenna with Adjustable Density Taper. *Int. J. Antennas Propag.* **2009**, *2009*, 624035. [CrossRef]
19. Gabrielli, L.H.; Hernandez-Figueroa, H.E. Aperiodic Antenna Array for Secondary Lobe Suppression. *IEEE Photon. Technol. Lett.* **2016**, *28*, 209–212. [CrossRef]
20. Martínez-Graullera, O.; Martín, C.J.; Godoy, G.; Ullate, L.G. 2D array design based on Fermat spiral for ultrasound imaging. *Ultrasonics* **2010**, *50*, 280–289. [CrossRef]
21. Juárez, E.; Panduro, M.A.; Reyna, A.; Covarrubias, D.H.; Mendez, A.; Murillo, E. Design of Concentric Ring Antenna Arrays Based on Subarrays to Simplify the Feeding System. *Symmetry* **2020**, *12*, 970. [CrossRef]
22. Cardoso, R.S.; Oliveira, L.P.; Hernandez-Figueroa, H.E. Assessment of Fermat's Spiral Arrays for Photonic Dielectric Antennas. In *Proceedings of the 2021 15th European Conference on Antennas and Propagation (EuCAP), Dusseldorf, Germany, 22–26 March 2021*; IEEE: New York, NY, USA, 2021; pp. 1–4. [CrossRef]
23. Betancourt, D.; del Rio Bocio, C. A Novel Methodology to Feed Phased Array Antennas. *IEEE Trans. Antennas Propag.* **2007**, *55*, 2489–2494. [CrossRef]
24. Ferrando, N.; Fonseca, N.J.G. Investigations on the Efficiency of Array Fed Coherently Radiating Periodic Structure Beam Forming Networks. *IEEE Trans. Antennas Propag.* **2011**, *59*, 493–502. [CrossRef]
25. Wen, Y.-Q.; Wang, B.-Z.; Ding, X. A Wide-Angle Scanning and Low Sidelobe Level Microstrip Phased Array Based on Genetic Algorithm Optimization. *IEEE Trans. Antennas Propag.* **2016**, *64*, 805–810. [CrossRef]
26. Juárez, E.; Panduro, M.A.; Covarrubias, D.H.; Reyna, A. Coherently Radiating Periodic Structures to Reduce the Number of Phase Shifters in a 2-D Phased Array. *Sensors* **2021**, *21*, 6592. [CrossRef]
27. Juarez, E.; Panduro, M.A.; Covarrubias, D.H.; Reyna, A.; Del Rio, C. Application of Coherently Radiating Periodic Structures for Feeding Subarrays in Limited-Scan Arrays. *IEEE Open J. Antennas Propag.* **2023**, *4*, 1154–1162. [CrossRef]
28. Juarez, E.; Mendoza, M.A.P.; Covarrubias, D.H.; Maldonado, A.R.; Sanchez, B.; del Rio, C. An Innovative Way of Using Coherently Radiating Periodic Structures for Phased Arrays with Reduced Number of Phase Shifters. *IEEE Trans. Antennas Propag.* **2022**, *70*, 307–316. [CrossRef]
29. Vogel, H. A better way to construct the sunflower head. *Math. Biosci.* **1979**, *44*, 179–189. [CrossRef]
30. Pita, J.L.; Aldaya, I.; Santana, O.J.S.; De Araujo, L.E.E.; Dainese, P.; Gabrielli, L.H. Side-lobe level reduction in bio-inspired optical phased-array antennas. *Opt. Express* **2017**, *25*, 30105–30114. [CrossRef] [PubMed]
31. Sadoc, J.-F.; Rivier, N.; Charvolin, J. Phyllotaxis: A non-conventional crystalline solution to packing efficiency in situations with radial symmetry. *Acta Crystallogr. Sect. A Found. Crystallogr.* **2012**, *68*, 470–483. [CrossRef]
32. Molnar, G.; Babic, M.; Sipus, Z. Closed-Form Design of Optimum Linear Arrays Based on Raised-Cosine Beampattern. In *Proceedings of the 2020 IEEE International Symposium on Antennas and Propagation and North American Radio Science Meeting, Montreal, QC, Canada, 5–10 July 2020*; IEEE: New York, NY, USA, 2020; pp. 1889–1890. [CrossRef]
33. Encino, K.; Panduro, M.A.; Reyna, A.; Covarrubias, D.H. Novel Design Techniques for the Fermat Spiral in Antenna Arrays, for Maximum SLL Reduction. *Micromachines* **2022**, *13*, 2000. [CrossRef]
34. Panduro, M.A.; Brizuela, C.A.; Balderas, L.I.; Acosta, D.A. A comparison of genetic algorithms, particle swarm optimization and the differential evolution method for the design of scannable circular antenna arrays. *Prog. Electromagn. Res. B* **2009**, *13*, 171–186. [CrossRef]
35. Bray, M.G.; Werner, D.H.; Boeringer, D.W.; Machuga, D.W. Optimization of thinned aperiodic linear phased arrays using genetic algorithms to reduce grating lobes during scanning. *IEEE Trans. Antennas Propag.* **2002**, *50*, 1732–1742. [CrossRef]
36. Panduro, M.A.; Brizuela, C.A.; Garza, J.; Hinojosa, S.; Reyna, A. A comparison of NSGA-II, DEMO, and EM-MOPSO for the multi-objective design of concentric rings antenna arrays. *J. Electromagn. Waves Appl.* **2013**, *27*, 1100–1113. [CrossRef]